JOURNAL OF CATALYSIS **161,** 230–246 (1996)
ARTICLE NO. 0181

Oxidation of Methanol over Polycrystalline Rh and Pt: Rates, OH Desorption, and Model

M. P. Zum Mallen[1] and L. D. Schmidt

Department of Chemical Engineering and Materials Science, University of Minnesota, Minneapolis, Minnesota 55455

Received September 18, 1995; revised February 1, 1996; accepted February 5, 1996

This paper extends previous mechanistic rate information for catalytic oxidation into a more complex fuel system, methanol oxidation over platinum and rhodium. Rh and Pt have generally similar characteristics, but also show some significant differences owing to the high energy binding state of oxygen on the rhodium surface. On Pt, previous catalyzed methanol oxidation research is examined and a mechanism involving surface carbon formation is proposed. Data over Pt metal from room temperature up to 1600 K is discussed. In general, methanol conversion starts at temperatures as low as 400 K in large excess oxygen, but begins at temperatures up to 900 K for methanol decomposition (no oxygen) on Pt. Evidence for a transition from a carbon covered to a CO covered surface with increasing temperature is examined. This transition results in low catalyst activity for decomposition below 900 K. Also, oscillatory behavior is noted in this system under some conditions. None of these effects are noted on Rh. In contrast to Pt, where oxygen improves low temperature conversion, a large excess of oxygen appears to block surface sites and reduce activity on Rh. Otherwise, Rh decomposes and oxidizes methanol without dissociating the C–O bond, leaving the metal active for decomposition at temperatures as low as 500 K. On both Pt and Rh, a mechanistic model is developed. These models give excellent agreement with experimental results, suggesting that the proposed mechanisms are at least qualitatively correct. On Rh, the model assumes noncompetitive oxygen binding and assumes the C–O bond to be nondissociative. On Pt, the model allows the methanol C–O bond to break, forming surface carbon. Other differences between Pt and Rh results can be readily attributed to differing activation barriers to hyroxyl formation on these two metals. © 1996 Academic Press, Inc.

INTRODUCTION

We have recently examined the catalytic oxidation of hydrogen on Pt and Rh using laser induced fluorescence (LIF) (1, 2) in order to obtain the elementary steps of this reaction. Now that we have built a foundation of mechanistic rate information for the catalytic oxidation of hydrogen, we can begin to examine more complicated fuel oxidation systems, such as methanol oxidation. On one hand, any attempt to kinetically model this reaction could quickly become problematic because of the number of possible reactions and variable parameters which need to be considered. On the other hand, we already have values for more than half of these parameters from the hydrogen oxidation system. We can thus treat these parameters as fixed and vary only the new mechanistic steps for methanol. In this manner, we can continually add to our knowledge of fuel oxidation systems.

There are several important reasons for the study of methanol as a fuel oxidation system. It is one of the largest volume commodity chemicals in the world with world production capacity in excess of 25 million tons (3). Methanol has many uses, including feedstock for other chemical production and for fuel cells. However, a fundamental understanding of catalytic decomposition and combustion of methanol is lacking.

There are several oxidation and decomposition pathways of methanol on Pt and Rh, the most important of which are summarized in Table 1. In this laboratory, Papapolymerou examined methanol decomposition on Pt (4). Others have considered methanol decomposition as well on Pt (5–11), Rh (12, 13), and Pd (14–22). Only one direct reference was found for steady-state methanol oxidation on Pt (23) and it was limited to highly fuel lean operation. We can, however, obtain indirect information through CO (24–27) and H_2 (26) oxidation on Pt.

OH radicals in methanol oxidation on metal catalysts have not been examined previously. Marks *et al.* (28) examined methane oxidation on Pt. This is not a particularly good indication of methanol behavior, however, because methane does not readily bind to noble metals, whereas the lone-pair oxygen electrons of methanol allow the molecule to adsorb readily. Methanol also provides some of its own oxygen for product formation because carbon monoxide forms under decomposition conditions, while methane requires C–O bond formation.

We will show that decomposition behavior is dominated by the breaking of the methanol C–O bond on Pt and formation of carbon on the low temperature Pt surface. This has the overall effect of keeping catalyst activity very low

[1] Present address: Union Carbide Corporation, 3333 South Highway 6, Houston, TX 77082.

0021-9517/96 $18.00

TABLE 1

Thermodynamics of Gas-Phase Methanol Oxidation

Reactants	Products	ΔH (kcal/mol)
$CH_3OH \rightarrow$	$CO + 2H_2$	21.66
	$H_2CO + H_2$	20.37
	$C + H_2O + H_2$	−9.70
$CH_3OH + 1/2\ O_2 \rightarrow$	$CO_2 + 2H_2$	−45.93
	$CO + H_2O + H_2$	−36.11
	$H_2CO + H_2O$	−37.39
	$C + 2H_2O$	−67.47
$CH_3OH + O_2 \rightarrow$	$CO_2 + H_2O + H_2$	−103.68
	$CO + 2H_2O$	−93.87
$CH_3OH + 3/2\ O_2 \rightarrow$	$CO_2 + 2H_2O$	−161.46

below 800 K. Above this temperature, steady-state surface carbon levels drop and methanol begins to decompose into CO and H_2. The addition of oxygen serves to reduce surface carbon levels and markedly increase catalytic activity, but it also affects the system by inducing unforced oscillatory behavior consistent with coverage shifts from a carbon to a CO covered surface.

In contrast, the methanol C–O bond remains essentially nondissociative at all temperatures on Rh and an activity loss is never noted on Rh. Rhodium also shows no indication of oscillatory behavior. This is consistent with our interpretation that these oscillations are induced by competition between a carbon site-blocking atom and an "active" methoxy or CO surface species. Because the methanol C–O bond appears to be nondissociative on Rh, no carbon is available to induce oscillations.

Oxygen binds far more strongly on Rh than on Pt, which results in a blocked Rh catalyst surface at high oxygen partial pressures. This is expected and consistent with results for hydrogen oxidation where high oxygen partial pressures yield competitive behavior between adsorbed O and other species on the surface. This can effectively slow down surface reactions.

Otherwise, the behavior of methanol oxidation on both metals was fairly as expected. We found that Rh desorbs much more H_2 and less H_2O than Pt under similar conditions. This is readily explained through the hydrogen oxidation pathways as shown previously (1) and summarized through the potential energy diagrams for methanol. This also indicates the role of hydrogen in methanol oxidation for both metals. Reaction energetics indicates that Rh would prefer to desorb hydrogen as H_2, whereas hydrogen will scavenge oxygen to form OH and H_2O on Pt.

EXPERIMENTAL

Details of the apparatus and experimental procedure have been described previously (1, 2). Briefly, the reaction chamber is a 0.4-liter stainless-steel six-way cross, mechanically pumped to achieve a base pressure below 10^{-3} Torr. Resistively heated catalytic foils, 0.17×3.0 cm, are suspended from leads and the surface temperature is monitored with a thermocouple. The total pressure was measured with a capacitance manometer, while partial pressures in reacting systems were measured by leaking into a turbomolecular pumped chamber equipped with a quadrupole mass spectrometer maintained at $\sim 10^{-8}$ Torr with appropriate calibrations and corrections for cracking in the mass spectrometer. In nonreacting systems and for calibrations, we measured partial pressures by differences in capacitance manometer measurements.

New catalyst foils were heated to high temperature (>1400 K) in oxygen for an extended period of time (typically 1 h) to remove any contaminants that may be present. The system was then cycled through several oxidation experiments to determine reproducibility. All experiments were preceded by a high temperature treatment of the catalytic foil in oxygen for several minutes to eliminate any contaminant build up (such as carbon). No changes in catalyst activity were noted with time on any surfaces. Results were repeated for at least four foils of each catalyst and runs on an "old" or used catalytic foil correlated very well with runs on a fresh foil.

Rates were measured using the continuous-stirred tank reactor (CSTR) equation. The CSTR assumption generally holds true for low pressure (below ~1.0 Torr) chambers because the reactor mixing time is much smaller than the average residence time.

For hydroxyl measurement, the Q_11 rotational line of the $^2A\Sigma^+ = {}^2X\Pi$ (307.844 nm) (29) transition was saturated by frequency doubling a tunable dye laser running at ~616 nm with Rhodamine 640 dye. The laser excitation source was a frequency doubled 10-Hz Q-switched pulsed Nd : YAG laser (532 nm output). The final dye laser beam passed <0.5 cm below the catalyst foil in the reaction chamber. Fluorescence measurements indicated that the system is fairly insensitive to laser beam position, any placement from 0.1 to 1.0 cm appeared to give experimentally equivalent results to within 10%. The fluorescence lifetime was measured to be >500 ns at 0.1 Torr, indicating negligible nonfluorescent decay, as expected from the low collision frequency at these pressures.

Fluorescent saturation conditions were used with typical laser energies of 500 μJ/pulse. The fluorescence signal was filtered and detected using a photomultiplier and a boxcar integrator which measured the fluorescence signal between 50 and 100 ns after the laser pulse. Data was usually taken by integrating 300 laser shots.

Throughout this paper, reactant chamber pressures are expressed as P and *initial* reactant partial pressures (without reaction) are given as P^{i}. P^{i} effectively expresses a constant feed rate of reactant into the reaction vessel and results in

reactant depletion as the reaction progresses. In oxidation situations it was necessary to use feed rates (P^i) because it was difficult to maintain constant oxygen and methanol partial pressures while varying temperature. Conversions ran as high as ~30%, but results were extrapolated to feed pressures for kinetic analysis.

RESULTS

Methanol Decomposition

Decomposition results for methanol on Rh and Pt are summarized in Fig. 1. Methanol decomposition on Rh (Fig. 1a) is generally similar to that on Pt (Fig. 1b); however, measurable conversion, as required by stoichiometry, begins at a significantly lower temperature on Rh (550 K) than on Pt (800 K). Conversion reaches a flux limited value at ~900 K on both metals. H_2 production follows the CO trend exactly and is not shown.

Results on Pt are consistent with previous Pt results by Papapolymerou *et al.* (4). Conversion of methanol remains approximately constant and therefore doubling methanol partial pressure yields approximately twice as much CO production. On Pt, at partial pressures above approximately 0.2 Torr, it was difficult to attain steady state and data were not reproducible. This is believed to be related to carbon formation on the Pt surface, as further indicated by XPS analysis which indicated that the inactive catalyst (700 K) contains over $2\frac{1}{2}$ times more carbon than a comparable active (1200 K) surface. This leads us to conclude that carbon is blocking the catalyst surface at lower temperatures. Further considerations of this are discussed later. This feature is not noted on Rh; the surface remains carbon free at all temperatures.

Overall, we observed ~30% methanol conversion to CO and H_2 at high temperatures on both metals and high temperatures (>1000 K). Also, CO production appears to be heavily suppressed on Pt until approximately 800 K.

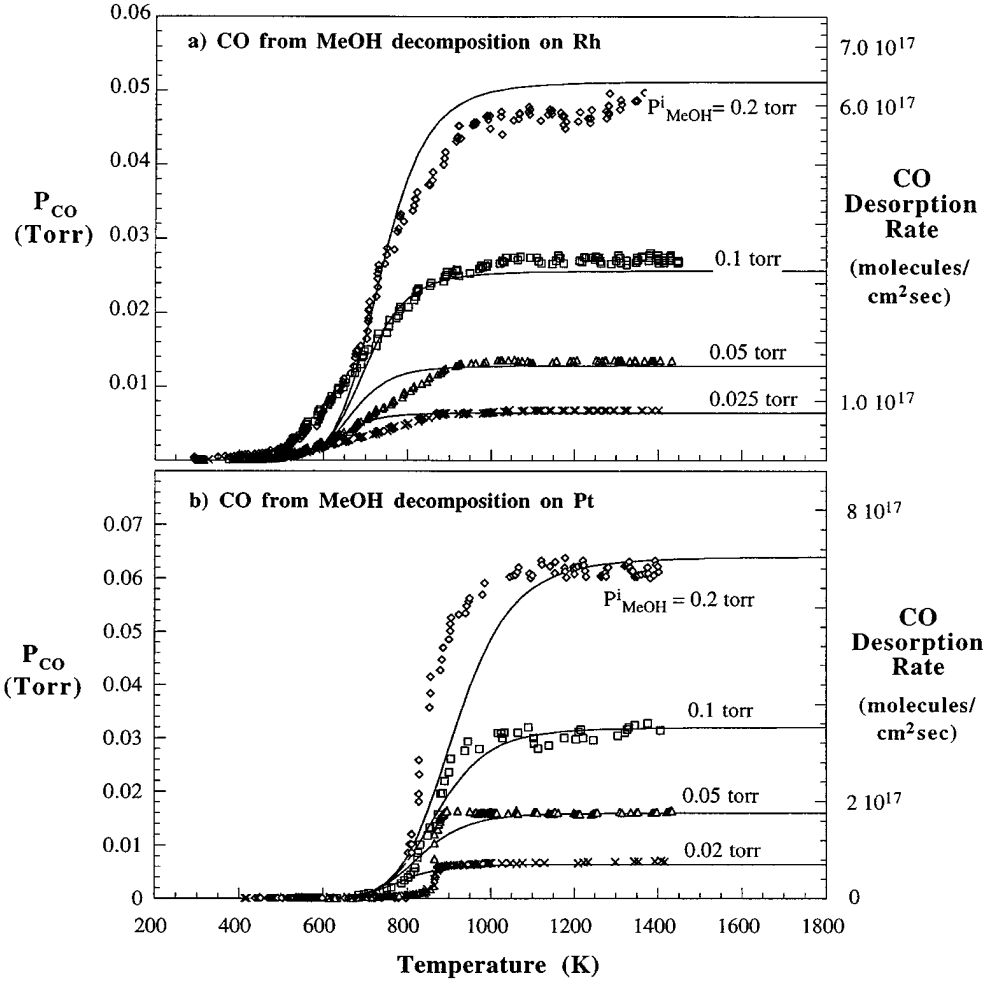

FIG. 1. Comparison of experimental results (points) and Langmuir–Hinshelwood fits (lines) for carbon monoxide production as a function of temperature from methanol decomposition on a polycrystalline (a) Rh and (b) Pt foil. H_2 production follows the same trend and is not shown. No products other than CO and H_2 are noted.

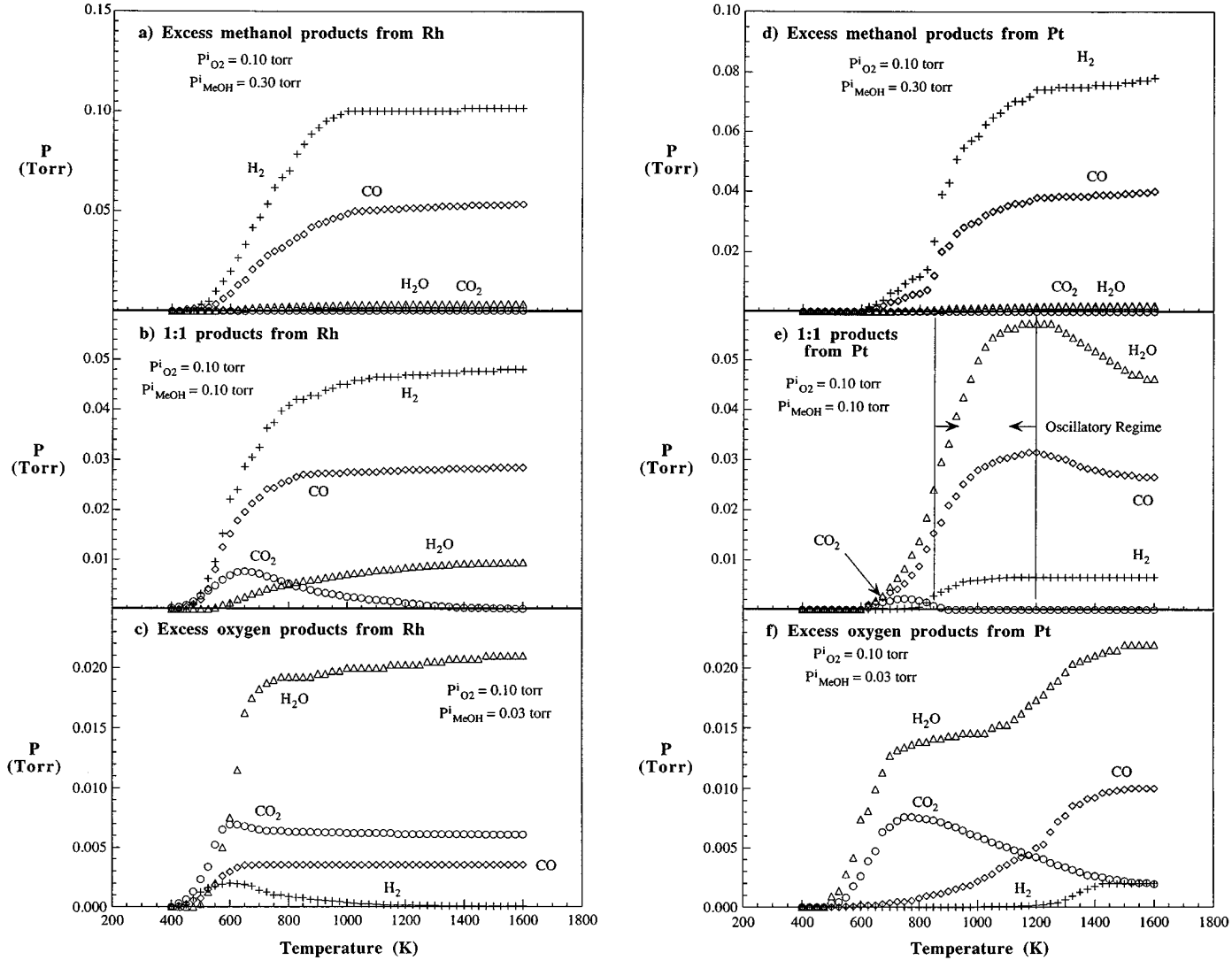

FIG. 2. Product partial pressures as a function of temperature for methanol oxidation on Rh in (a) excess methanol, (b) an equal inlet mixture of methanol and oxygen, and (c) excess oxygen. (d–f) Similar results for Pt. Note, (e) can show oscillatory behavior; results shown are without oscillation.

Above this temperature, methanol quickly decomposes and reaches a value limited by the flux of methanol vapor to the catalyst surface.

Neither Pt nor Rh showed OH desorption for methanol decomposition. This is consistent with mass balance considerations on the system. Any oxygen which forms OH will lead to carbon atom formation which would in turn deactivate the surface.

Methanol Oxidation

Stable products formed in methanol oxidation on Rh and Pt are summarized in Fig. 2. Three compositions are shown for each metal: excess methanol, excess oxygen, and a 1 : 1 (equimolar) inlet of reactants. For all product partial pressures, mass balances of C, H, and O closed to within 10%.

There are several interesting features of these results. First, on Rh, we see that H_2O and CO_2 are the primary products in excess oxygen (Fig. 2c), but that a large amount of H_2 desorbs at low temperatures even under these conditions. Equal ratios of methanol and oxygen (Fig. 2b) strongly favor H_2 (six times more hydrogen than water), excess methanol (Fig. 2a) yields hydrogen and CO almost exclusively. Essentially no water or CO_2 is seen in excess methanol and the reaction closely mimics the behavior seen for pure methanol decomposition, as expected.

An analysis of product concentrations over the same range of methanol and oxygen partial pressures on Pt reveals some additional information. First, in strong excess methanol (Fig. 2d), we see hydrogen and CO as our primary products, as we would expect. Water and CO_2 are strongly suppressed, as is *all* product evolution below ~600 K. The

presence of oxygen *does* open the Pt catalyst up to some reaction below 800 K, however. In contrast, this is not seen in the strict decomposition reaction (Fig. 1b) due to carbon formation. Strong excess oxygen (Fig. 2f) favors water and CO_2 desorption at lower temperatures (below 1100 K). Higher temperatures result in increased conversion of methanol, additional water, and a reduction of CO_2 in favor of CO desorption. The complete oxidation products ($CO_2 + H_2O$) differ from partial oxidation products substantially in that they tend to develop their peak product at very low temperature (<550 K). In excess oxygen, CO and H_2 production are completely suppressed in favor of complete oxidation below 1200 K.

Perhaps the most interesting results on Pt come from approximately equal partial pressures of methanol and oxygen (Fig. 2e) where we find somewhat surprisingly that water and carbon monoxide are the two major products. Note that a 1 : 1 methanol : oxygen ratio is deficient in O_2 for complete combustion, but we might expect CO_2, H_2O, and H_2 as major products, not H_2O and CO. We will consider this further in the discussion. Furthermore, the minor CO_2 and H_2 peaks (<10% of major products) indicate that total oxidation products are favored at lower temperatures, followed by decomposition products as the reaction temperature exceeds 800 K. Note also that Pt can show oscillations under these specific conditions, but the results shown are *without* oscillations. The observed reactant and product partial pressures vary substantially with oscillation, however, as shown in Fig. 3 and discussed below.

Figure 4a shows OH desorption rate in 0.1 Torr O_2 with variation in methanol partial pressure (0.0–0.2 Torr) on Rh. Four temperatures are shown, and we can see that peak OH production occurs at low CH_3OH/O_2 ratio (0.01 Torr methanol) similar to hydrogen oxidation (1). This peak is followed by a gradual decrease back to the baseline at 0.1–0.15 Torr methanol.

Figure 4b shows OH Arrhenius plots for 0.005–0.050 Torr methanol in 0.1 Torr oxygen on Pt. All four methanol partial pressures yield an *apparent* E_{dOH} of ~20 kcal/mol, constrained by our detection limits at low temperatures and flux limitations at high temperatures.

In all oxidation cases on both Pt and Rh, the O_2 conversion remains quite low. An excess of methanol tends to lead to greater partial oxidation (CO and H_2) production so large oxygen conversions never occur. The maximum oxygen conversion observed on Pt was ~0.25 (at 1 : 1 $O_2 : CH_3OH$); it was 0.12 on Rh (in excess O_2). The maximum methanol conversion was ~0.30 on both metals.

Oscillations

One interesting observation in methanol oxidation on Pt is that oscillations occurred under certain conditions. Oscillations are found in temperature, reactant, and product partial pressures, and they generally occur between 0.05 and 0.2 Torr methanol in 0.1 Torr oxygen and temperatures from 900 to 1100 K.

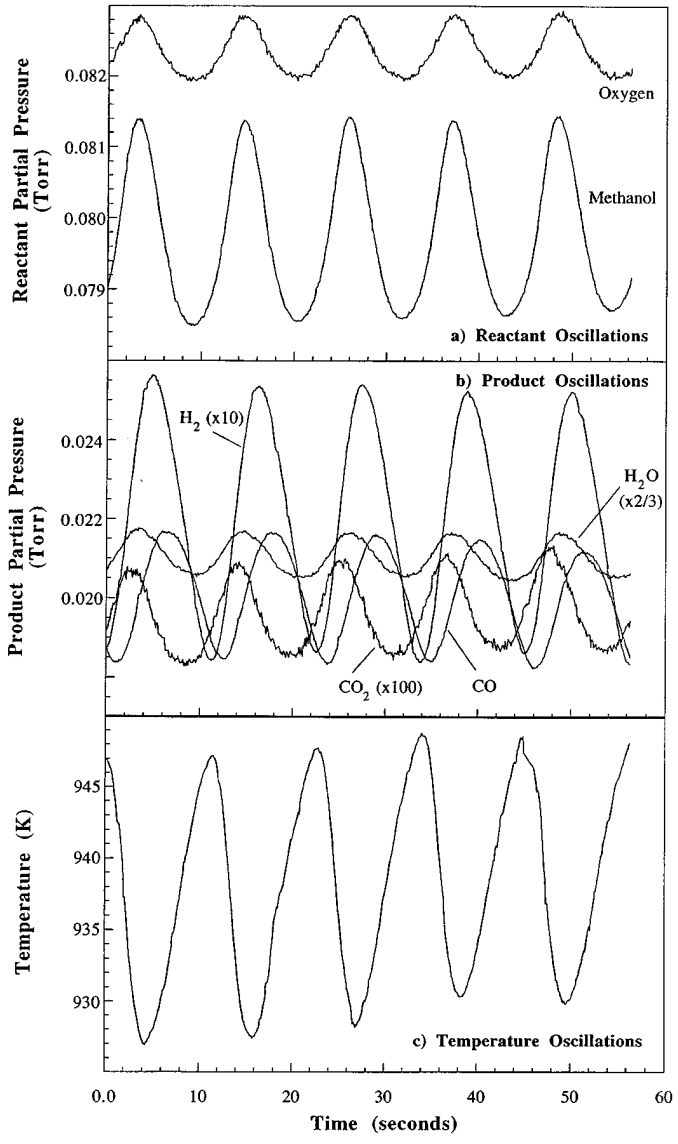

FIG. 3. Oscillations in time during methanol oxidation on Pt. $P^i(MeOH) = P^i(O_2) = 0.1$ Torr. (a) Variations in reactant partial pressure with time. (b) Variations in products partial pressure with time (note multiplicative factors). (c) Temperature oscillations. Results are for constant reactant flow rates and foil power input.

Results for 0.1 Torr methanol and 0.1 Torr oxygen are illustrated in Fig. 3. The temperature measurement (via thermocouple attached to the foil surface) tends to *lead* partial pressure readings by about 4 s or about $\frac{1}{3}$ phase. This is not unexpected because we are operating in a CSTR, and therefore we observe an inherent time delay for changes in product pressure, while the thermocouple gives an instantaneous temperature measurement.

Based on this, we can see that the reactants methanol and oxygen, as well as the *complete* combustion products CO_2

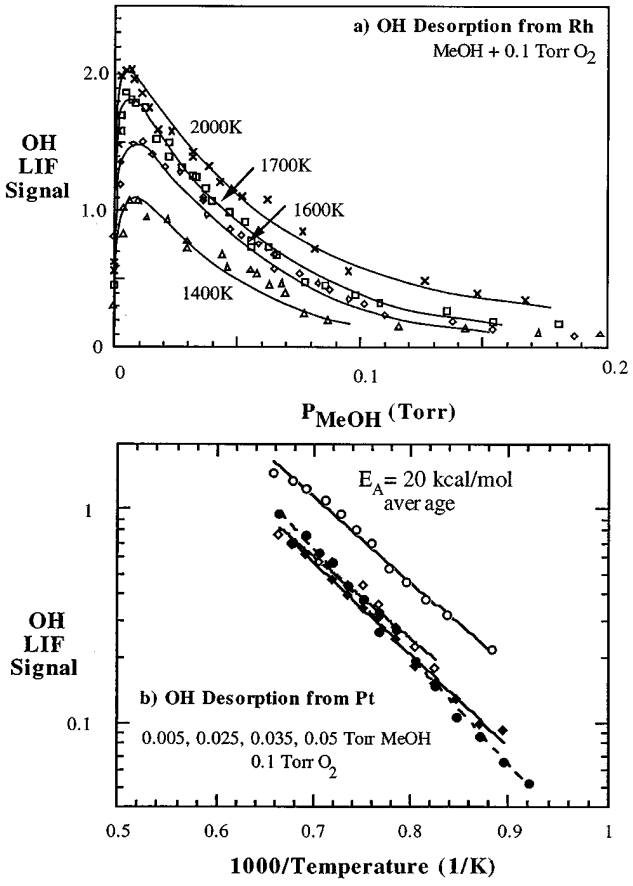

FIG. 4. (a) Experimental results of OH desorption rate as a function of methanol pressure in 0.1 Torr O_2 over a Rh catalyst. (b) Experimental results for OH desorption rate as a function of reciprocal temperature during methanol oxidation on Pt. Results are for 0.005 (open circles), 0.025 (closed circles), 0.035 (open diamonds), and 0.050 (closed diamonds) Torr methanol and 0.1 Torr O_2. Apparent activation energy is ~20 kcal/mol in each Pt case.

and H_2O all follow the temperature curve exactly, showing that the maximum in complete combustion products occurs at the maximum in temperature. This is expected, given the exothermicity of the complete combustion reaction.

In contrast, the methanol decomposition products ($CO + H_2$) *lag* the other products by $\sim\frac{1}{4}$ phase. This is also expected because the peaks in decomposition products occur as the temperature drops down to its low point. The lowered temperature is indicative of the endothermic methanol decomposition reaction occurring.

It is somewhat surprising that methanol and oxygen reach their peak partial pressure concurrently with the CO_2 and H_2O product peaks. We might expect that increased total oxidation production correlates to decreased reactant concentration. Actually, the system is still somewhat fuel rich at this ratio and thus the maximum production of *decomposition* products (not oxidation) should correlate to the minimum in methanol. In the discussion, we will also consider the possibility that the catalyst surface is significantly *less* active when CO_2 and H_2O is desorbed to yield an overall increase in gas-phase reactant concentrations.

MODEL

By combining our previous knowledge of hydrogen oxidation on Pt (2) and Rh (1) with the additional information presented here, we will attempt to estimate surface kinetic parameters and activation energies of intermediate surface steps. Unlike our previous work on hydrogen oxidation, the methanol mechanism contains a large number of steps and can quickly become intractable. For this reason, the model has intentionally been made as simple as possible. Specifically, all Rh reaction pathways are assumed to proceed through methanol decomposition where methanol first dissociates on the surface to CO and hydrogen which may subsequently desorb or combine with oxygen to yield CO_2, OH, and/or H_2O. This mechanism, coupled with our previous knowledge of hydrogen oxidation, provides a workable framework for examining experimental data. We should point out, however, that this approach provides only a very simplified first approach to describing this system. As we will consider later, more complex steps could be added to improve model fits.

Overall, two separate models were examined for suitability in the methanol system on Rh and Pt. The mechanism and notation used for Rh are

$$CH_3OH_{(g)} \underset{k_{dM}}{\overset{k_{aM}}{\rightleftarrows}} CH_3OH_{(a)} \quad [1]$$

$$O_{2(g)} \underset{k_{dO}}{\overset{k_{aO}}{\rightleftarrows}} 2O_{(a)} \quad [2]$$

$$2H_{(a)} \xrightarrow{k_{dH}} H_{2(g)} \quad [3]$$

$$H_2O_{(a)} \xrightarrow{k_{dW}} H_2O_{(g)} \quad [4]$$

$$CO_{(a)} \xrightarrow{k_{dCO}} CO_{(g)} \quad [5]$$

$$OH_{(a)} \xrightarrow{k_{dOH}} OH_{(g)} \quad [6]$$

for rates of adsorption/desorption and

$$H_{(a)} + O_{(a)} \underset{k_{-1}}{\overset{k_1}{\rightleftarrows}} OH_{(a)} \quad [7]$$

$$H_{(a)} + OH_{(a)} \underset{k_{-2}}{\overset{k_2}{\rightleftarrows}} H_2O_{(a)} \quad [8]$$

$$CH_3OH_{(a)} \xrightarrow{k_4} CO_{(a)} + 4H_{(a)} \quad [9]$$

$$CO_{(a)} + O_{(a)} \xrightarrow{k_5} CO_{2(g)} \quad [10]$$

for the surface reactions. This model is fairly compact with

TABLE 2

Parameters (Preexponentials and Activation Energies) for the Mechanistic Steps in the Pt and Rh Methanol Oxidation Models

Reaction		Rhodium			Platinum		
		Preexponential ($Torr^{-1}\ s^{-1}, s^{-1}$)	Activation energy (kcal/mol)	References	Preexponential ($Torr^{-1}\ s^{-1}, s^{-1}$)	Activation energy (kcal/mol)	References
$H_{(a)} + O_{(a)} \xrightarrow{k_1} OH_{(a)}$	(1)	7×10^{12}	20	Zum Mallen *et al.* (1)	1×10^{15}	2.5	Williams *et al.* (2)
$OH_{(a)} \xrightarrow{k_{-1}} H_{(a)} + O_{(a)}$	(−1)	—	0	Zum Mallen *et al.* (1)	1×10^{8}	5	Williams *et al.* (2)
$H_{(a)} + OH_{(a)} \xrightarrow{k_2} H_2O_{(a)}$	(2)	3×10^{17}	8	Zum Mallen *et al.* (1)	9×10^{16}	15.3	Williams *et al.* (2)
$H_2O_{(a)} \xrightarrow{k_{-2}} H_{(a)} + OH_{(a)}$	(−2)	5×10^{14}	42	Zum Mallen *et al.* (1)	1.8×10^{13}	36.8	Williams *et al.* (2)
$CH_3OH_{(a)} \xrightarrow{k_4} CO_{(a)} + 4H_{(a)}$	(4 : Rh)	1×10^{14}	12	This work	—	—	—
$CH_3OH_{(a)} \xrightarrow{k_4} C_{(a)} + O_{(a)} + 4H_{(a)}$	(4 : Pt)	—	—	—	1×10^{10}	11	This work
$CO_{(a)} + O_{(a)} \xrightarrow{k_5} CO_{2(g)}$	(5)	1×10^{10}	25	Campbell *et al.* (44)	1×10^{15}	24.1	Campbell *et al.* (25)
$C_{(a)} + O_{(a)} \xrightarrow{k_6} CO_{(a)}$	(6)	—	—	—	5×10^{13}	15	Hickman and Schmidt (49)
$CH_3OH_{(g)} \xrightarrow{k_{aM}} CH_3OH_{(a)}$	(M)	3.5×10^5 ($S_M = 1.0$)	0	This work	3.5×10^5 ($S_M = 1.0$)	0	This work
$CH_3OH_{(a)} \xrightarrow{k_{dM}} CH_3OH_{(g)}$	(−M)	1×10^{13}	11	Parmeter *et al.* (12)	1×10^{13}	11	Sexton *et al.* (50)
$O_{2(g)} \xrightarrow{k_{aO}} O_{(a)}$	(O)	3.5×10^5 ($S_o = 1.0$)	0	Zum Mallen *et al.* (1)	1×10^4 ($S_o = 0.02$)	0	Williams *et al.* (2)
$O_{(a)} \xrightarrow{k_{dO}} O_{2(g)}$	(−O)	1×10^{13}	70	Matsushima (40)	1×10^{13}	52	Matsushima (40)
$H_{(a)} \xrightarrow{k_{dH}} H_{2(g)}$	(−H)	1×10^{13}	18	Yates *et al.* (45)	1×10^{13}	18	McCabe and Schmidt (51)
$H_2O_{(a)} \xrightarrow{k_{dW}} H_2O_{(g)}$	(−W)	1×10^{13}	10.8	Kiss and Solymosi (46) Wagner and Moylan (47)	1×10^{13}	10.8	Fisher and Gland (52)
$CO_{(a)} \xrightarrow{k_{dCO}} CO_{(g)}$	(−CO)	1×10^{13}	32	Thiel *et al.* (48)	1×10^{13}	30	Seebauer *et al.* (33) MsCabe and Schmidt (51)
$OH_{(a)} \xrightarrow{k_{dOH}} OH_{(g)}$	(−OH)	8.1×10^{11}	34	Zum Mallen *et al.* (1)	1.5×10^{13}	48	Williams *et al.* (2)

kinetic information that is generally known. Overall, this mechanism has 14 individual steps, but 9 of these parameters (the adsorption/desorption steps for hydrogen, oxygen, water, and hydroxyl as well as Reaction steps (±1) and(±2)) are already fixed by our previous work on hydrogen oxidation. Four more parameters are set by the literature, leaving only one reaction step (k_4) to adjust for model fits. These results are summarized in Table 2 and provide the fits for methanol decomposition oxidation on a Rh surface. We believe that these curve fits are quite good, particularly since they have predictive value over temperatures ranging from 400 to 1600 K, a range in which the catalyst goes from 1.0 to $<10^{-6}$ Langmuir coverage. Furthermore, we are using a single set of mechanistic rate parameters for *all* of the Rh data presented, including later oxidation results.

At lower temperatures this reaction set was not adequate for Pt. As shown above, we observed a significant carbon buildup and deactivation on the low temperature Pt surface, a phenomena which was not observed on Rh where the methanol C–O bond is completely nondissociative. We therefore extended the model parameters slightly to allow for carbon formation on the catalyst surface, modifying reaction (k_4) to

$$CH_3OH_{(a)} \xrightarrow{k_4} C_{(a)} + O_{(a)} + 4H_{(a)} \qquad [11]$$

and adding reaction (k_6)

$$C_{(a)} + O_{(a)} \xrightarrow{k_6} CO_{(a)}. \qquad [12]$$

Using this 15-parameter set of rates for this reaction (summarized in Table 2), we find reasonable agreement between model and essentially all experimental Pt results. Note that reaction mechanism (±3) is absent from both mechanisms as it was defined in our previous hydrogen oxidation model ($2OH \leftrightarrow O + H_2O$) (1, 2). This was a minor route for hydrogen oxidation, and our model is fairly

insensitive to the value of this parameter; we therefore omitted it from the methanol oxidation models. We leave reaction term (±3) unused in this paper to avoid confusion with prior definition.

These mechanisms provided the basic framework for examining the Rh and Pt reaction systems. A total of seven surface species are considered, and model results are generated by simultaneously considering steady-state coverage balances on each species from mass balance equations,

$$\frac{d\theta_{\mathrm{MeOH}}}{dt} = 0 = k_{\mathrm{aM}}\theta_{\mathrm{V}}P_{\mathrm{MeOH}} - k_{\mathrm{dM}}\theta_{\mathrm{MeOH}} - k_4\theta_{\mathrm{MeOH}}\theta_V^5 \quad [13]$$

$$\frac{d\theta_{\mathrm{o}}}{dt} = 0 = nk_{\mathrm{aO}}\theta_{\mathrm{V}}^n P_{\mathrm{O_2}} + k_{-1}\theta_{\mathrm{OH}}\theta_{\mathrm{V}} + k_4\theta_{\mathrm{MeOH}}\theta_{\mathrm{V}}^5 - nk_{\mathrm{dO}}\theta_{\mathrm{O}}^n - k_1\theta_{\mathrm{H}}\theta_{\mathrm{O}} - k_5\theta_{\mathrm{CO}}\theta_{\mathrm{O}} - k_6\theta_{\mathrm{C}}\theta_{\mathrm{O}} \quad [14]$$

$$\frac{d\theta_{\mathrm{H_2O}}}{dt} = 0 = k_2\theta_{\mathrm{H}}\theta_{\mathrm{OH}} - k_{-2}\theta_{\mathrm{H_2O}}\theta_{\mathrm{V}} - k_{\mathrm{dW}}\theta_{\mathrm{H_2O}} \quad [15]$$

$$\frac{d\theta_{\mathrm{CO}}}{dt} = 0 = k_6\theta_{\mathrm{C}}\theta_{\mathrm{O}} - k_{\mathrm{dCO}}\theta_{\mathrm{CO}} - k_5\theta_{\mathrm{CO}}\theta_{\mathrm{O}} \quad [16]$$

$$\frac{d\theta_{\mathrm{H}}}{dt} = 0 = 4k_4\theta_{\mathrm{MeOH}}\theta_{\mathrm{V}}^5 + k_{-1}\theta_{\mathrm{OH}}\theta_{\mathrm{V}} + k_{-2}\theta_{\mathrm{H_2O}}\theta_{\mathrm{V}} - nk_{\mathrm{dH}}\theta_{\mathrm{H}}^n - k_1\theta_{\mathrm{H}}\theta_{\mathrm{O}} - k_2\theta_{\mathrm{H}}\theta_{\mathrm{OH}} \quad [17]$$

$$\frac{d\theta_{\mathrm{OH}}}{dt} = 0 = k_1\theta_{\mathrm{H}}\theta_{\mathrm{O}} + k_{-2}\theta_{\mathrm{H_2O}}\theta_{\mathrm{V}} - k_{\mathrm{dOH}}\theta_{\mathrm{OH}} - k_{-1}\theta_{\mathrm{OH}}\theta_{\mathrm{V}} - k_2\theta_{\mathrm{H}}\theta_{\mathrm{OH}} \quad [18]$$

$$\frac{d\theta_{\mathrm{C}}}{dt} = 0 = k_4\theta_{\mathrm{MeOH}}\theta_{\mathrm{V}}^5 - k_6\theta_{\mathrm{C}}\theta_{\mathrm{O}}, \quad [19]$$

where

$$\theta_{\mathrm{V}} = 1 - \theta_{\mathrm{MeOH}} - \theta_{\mathrm{O}} - \theta_{\mathrm{H_2O}} - \theta_{\mathrm{CO}} - \theta_{\mathrm{H}} - \theta_{\mathrm{OH}} - \theta_{\mathrm{C}} \quad [20]$$

and n is the order of adsorption/desorption for H and O.

Rather than attempt to maintain a constant reactant partial pressure with reactions in progress, it is preferable to hold a constant inlet feed of reactants. Therefore, the model also calculates CSTR reactor pressures of oxygen and methanol, give the inlet pressures

$$\frac{\left(P_{\mathrm{O_2}}^{\mathrm{i}} - P_{\mathrm{O_2}}\right)V_{\mathrm{r\times r}}N_{\mathrm{av}}}{\tau_{\mathrm{O_2}}A_{\mathrm{surface}}\mathrm{RT_g}} + N_{\mathrm{o}}(n/2)\left(k_{\mathrm{dO}}\theta_{\mathrm{O}}^n - k_{\mathrm{aO}}\theta_{\mathrm{V}}^n P_{\mathrm{O_2}}\right) = 0 \quad [21]$$

$$\frac{\left(P_{\mathrm{MeOH}}^{\mathrm{i}} - P_{\mathrm{MeOH}}\right)V_{\mathrm{r\times r}}N_{\mathrm{av}}}{\tau_{\mathrm{MeOH}}A_{\mathrm{surface}}\mathrm{RT_g}} + N_{\mathrm{o}}(k_{\mathrm{dM}}\theta_{\mathrm{MeOH}} - k_{\mathrm{aM}}\theta_{\mathrm{V}}P_{\mathrm{MeOH}}) = 0 \quad [22]$$

where $V_{\mathrm{r\times r}}$ is the reactor volume, A_{surface} is the catalyst surface area, T_{g} is the gas phase temperature, τ is species residence time and N_{o} is monolayer coverage in molecules/cm^2.

Equations [13] through [22] form a system of 10 equations with 10 unknowns (P_{MeOH}, $P_{\mathrm{O_2}}$, θ_{V}, θ_{MeOH}, θ_{O}, $\theta_{\mathrm{H_2O}}$, θ_{CO}, θ_{C}, θ_{H}, and θ_{OH}), three experimentally fixed parameters ($P_{\mathrm{MEOH}}^{\mathrm{i}}$, $P_{\mathrm{O_2}}^{\mathrm{i}}$, and T_{s}), and 15 adjustable parameters (k_i). As mentioned above, however, many of these adjustable parameters (9) can be fixed by our previous work on hydrogen oxidation. Desorption rates are calculated as a function of species coverage and Arrhenius (temperature) dependent activation energy.

For Rh, the mass balance equations are fairly analogous to those for Pt with the exception of the nondissociative methanol C–O bond. Implementation of these rate steps is somewhat different from that for Pt, however, because there are two oxygen binding states on Rh, competitive and noncompetitive, as considered previously (1). Briefly, we found that oxygen on Rh binds in two distinct states (25 and 85 kcal/mol). Prior research has shown that the high-energy oxygen binding state is noncompetitive with other adsorbed species, although oxygen in the 25-kcal state does block surface sites (or compete) (30, 31). Therefore, the steady-state coverages for methanol oxidation (Eqs. [13] to [22]) were modified to account for competitive and noncompetitive oxygen species as well as nondissociative C–O bonding,

$$\frac{d\theta_{\mathrm{MeOH}}}{dt} = 0 = k_{\mathrm{aM}}\theta_{\mathrm{V}}P_{\mathrm{MeOH}} - k_{\mathrm{dM}}\theta_{\mathrm{MeOH}} - k_4\theta_{\mathrm{MeOH}}\theta_{\mathrm{V}}^4 \quad [23]$$

$$\frac{d\boldsymbol{\theta}_{\mathrm{o}}^{(\mathrm{NC})}}{dt} = 0 = nk_{\mathrm{aO}}\left(\boldsymbol{\theta}_{\mathrm{v}}^{(\mathrm{NC})}\right)^n P_{\mathrm{O_2}} + k_{-1}\theta_{\mathrm{OH}}\boldsymbol{\theta}_{\mathrm{v}}^{(\mathrm{NC})} - nk_{\mathrm{dO}}\left(\boldsymbol{\theta}_{\mathrm{o}}^{(\mathrm{NC})}\right)^n - k_1\theta_{\mathrm{H}}\boldsymbol{\theta}_{\mathrm{o}}^{(\mathrm{NC})} - k_5\theta_{\mathrm{CO}}\boldsymbol{\theta}_{\mathrm{o}}^{(\mathrm{NC})} \quad [24]$$

$$\frac{d\theta_{\mathrm{H_2O}}}{dt} = 0 = k_2\theta_{\mathrm{H}}\theta_{\mathrm{OH}} - k_{-2}\theta_{\mathrm{H_2O}}\theta_{\mathrm{V}} - k_{\mathrm{dW}}\theta_{\mathrm{H_2O}} \quad [25]$$

$$\frac{d\theta_{\mathrm{CO}}}{dt} = 0 = k_4\theta_{\mathrm{MeOH}}\theta_{\mathrm{V}}^4 - k_{\mathrm{dCO}}\theta_{\mathrm{CO}} - k_5\theta_{\mathrm{CO}}\boldsymbol{\theta}_{\mathrm{o}}^{(\mathrm{NC})} \quad [26]$$

$$\frac{d\theta_{\mathrm{H}}}{dt} = 0 = 4k_4\theta_{\mathrm{MeOH}}\theta_{\mathrm{V}}^4 + k_{-1}\theta_{\mathrm{OH}}\theta_{\mathrm{V}} + k_{-2}\theta_{\mathrm{H_2O}}\theta_{\mathrm{V}} - nk_{\mathrm{dH}}\theta_{\mathrm{H}}^n - k_1\theta_{\mathrm{H}}\boldsymbol{\theta}_{\mathrm{o}}^{(\mathrm{NC})} - k_2\theta_{\mathrm{H}}\theta_{\mathrm{OH}} \quad [27]$$

$$\frac{d\theta_{\mathrm{OH}}}{dt} = 0 = k_1\theta_{\mathrm{H}}\boldsymbol{\theta}_{\mathrm{o}}^{(\mathrm{NC})} + k_{-2}\theta_{\mathrm{H_2O}}\theta_{\mathrm{V}} - k_{\mathrm{dOH}}\theta_{\mathrm{OH}} - k_{-1}\theta_{\mathrm{OH}}\theta_{\mathrm{V}} - k_2\theta_{\mathrm{H}}\theta_{\mathrm{OH}}, \quad [28]$$

where

$$\theta_{\mathrm{V}} = 1 - \theta_{\mathrm{MeOH}} - f\boldsymbol{\theta}_{\mathrm{o}}^{(\mathrm{NC})} - \theta_{\mathrm{H_2O}} - \theta_{\mathrm{CO}} - \theta_{\mathrm{H}} - \theta_{\mathrm{OH}} \quad [29]$$

and the coverage of non-competitive oxygen vacant sites is

$$\boldsymbol{\theta}_{\mathrm{V}}^{(\mathrm{NC})} = 1 - \boldsymbol{\theta}_{\mathrm{o}}^{(\mathrm{NC})} \quad [30]$$

These equations are coupled with two CSTR species balances similar to Eqs. [21] and [22] above.

As indicated in a previous paper, f is the oxygen binding state ratio ($\theta_O/\boldsymbol{\theta}_o^{(NC)}$) and can be expressed exclusively in terms of $\boldsymbol{\theta}_o^{(NC)}$ and $K_{o(a)}$, the equilibrium condition for adsorbed oxygen (1). Equations [21] through [30] form the Rh system of 10 equations with 10 unknowns (θ_V, $\boldsymbol{\theta}_v^{(NC)}$, θ_{MeOH}, $\boldsymbol{\theta}_o^{(NC)}$, θH_2O, θ_{CO}, θ_H, θ_{OH}, P_{MeOH}, and P_{O_2}) three experimentally fixed parameters ($P^i_{O_2}$, P^i_{MeOH}, and T_s), and 14 adjustable parameters (k_i). Nine of the 14 adjustable parameters can be fixed, however, by our previous work on hydrogen oxidation and many others can be fixed by other literature. Thus the extremely complicated MeOH system will be reduced to 5 adjustable parameters by our previous knowledge and further reduced to 1 adjustable parameter by known literature values.

Although an additional complexity has been added over the Pt model due to the noncompetitive nature of adsorbed oxygen, the Rh model still remains mechanistically simpler than the model used for Pt. It is apparent that we could readily modify this model (given by Eqs. [1] to [10] by adding carbon as a surface species (Eqs.) [11] and [12] and modifying our mass balances correspondingly. In the Rh system, however, there is no indication that carbon exists as a major product on the catalyst. In fact, our experimental evidence supports the methanol C–O bond being essentially nondissociative on Rh. Any C–O bond breakage would eventually lead to surface carbon build up (during methanol decomposition), which is not seen experimentally. This is considered further in the discussion.

The Rh and Pt methanol oxidation models are both illustrated in Fig. 5. As we will show, these mechanisms offer reasonable agreement with essentially all of our experimental data.

Model parameters for both systems are listed in Table 2. For most parameters,the values follow directly from our previous hydrogen oxidation work on Pt (2) and Rh (1). Otherwise, data come from the literature where available.

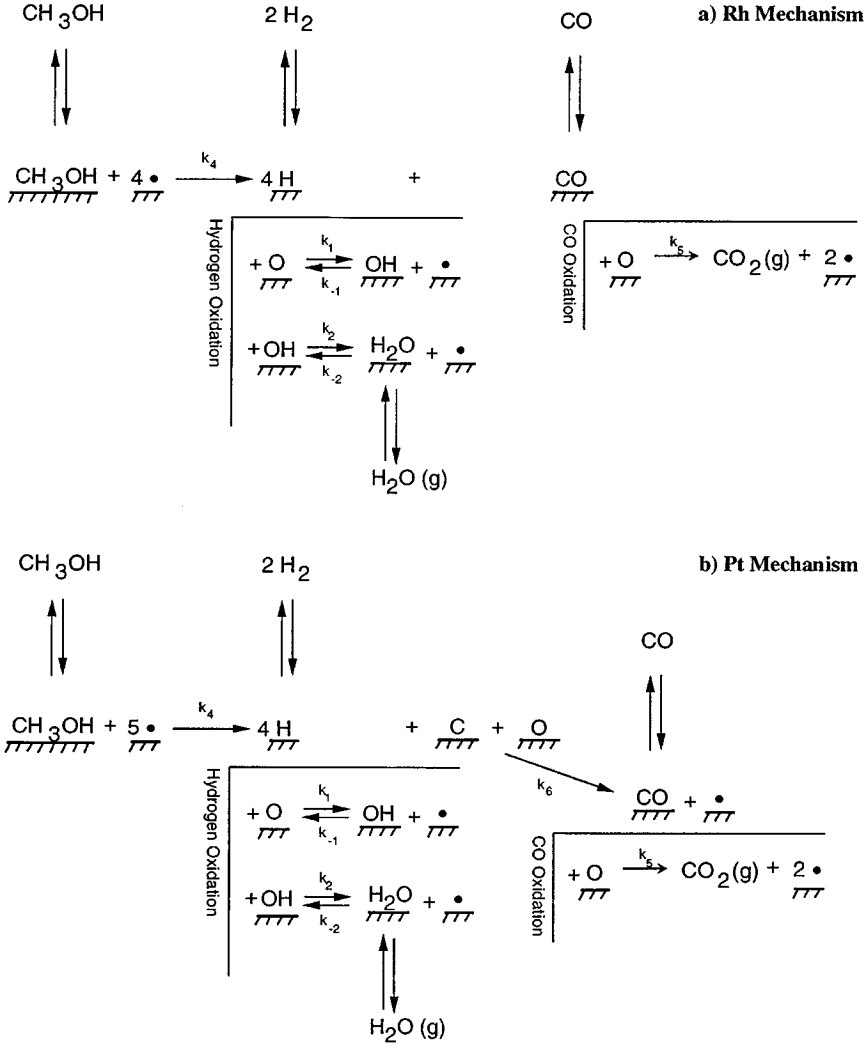

FIG. 5. Reaction mechanisms used in modeling the (a) Rh and (b) Pt methanol system. The bullets indicate vacant surface sites.

Exceptions are the adsorption of reactants (methanol and oxygen), whose values are calculated as a flux to the surface and assume a nonactivated adsorption process given as

$$k_a = \frac{S}{\sqrt{2\pi m R T_g}} \qquad [31]$$

and the value of surface reaction step k_4 which is varied to achieve reasonable agreement with the experimental results.

Numerical Results

Methanol decomposition. Predicted methanol decomposition is shown along with the experimental results in Fig. 1. The model gives good qualitative agreement. Specifically, on Rh it shows limited activity below 550 K, but then an increase to the flux limit at about 900 K. This is completely consistent with experiments. Calculated coverages (not shown) indicate that adsorbed carbon monoxide is primarily responsible for reduced catalyst activity at lower temperatures because of its high coverage on Rh. This is expected because CO desorption has the largest activation barrier (32 kcal/mol) of the possible species present in the absence of O_2. H_2 and methanol offer substantially lower desorption barriers at 18 and 11 kcal/mol, respectively, and have correspondingly lower coverages on the Rh surface. This can be directly contrasted with decomposition on Pt (Fig. 1b) where carbon formation causes catalyst deactivation even up to 800 K. This adds evidence to carbon formation on Pt rather than CO. If CO were poisoning the Pt surface, we would see desorption beginning at 600 K, similar to that seen with Rh, since CO has a similar desorption activation barrier on both metals (30 versus 32 kcal/mol). Actual product formation on Pt is strongly inhibited below 800 K. Note that, unlike a Langmuir–Hinshelwood expression, the model considers rates of *all* competing reactions simultaneously and does not require adsorption–desorption equilibrium. Furthermore, steady-state carbon coverages become high at lower temperatures on Pt, consistent with what we have shown experimentally during methanol decomposition.

Methanol oxidation. The model predicted stable product desorption from methanol oxidation is shown in Fig. 6. Overall, the mechanism predicts oxidation behavior fairly well and illustrates significant differences between Rh and Pt. Figure 6a shows products over Rh. For CO_2, the temperature placement of the peak and fairly slow decrease at high temperatures is consistent with experimental results (Fig. 2b), although model desorption is enhanced by a factor

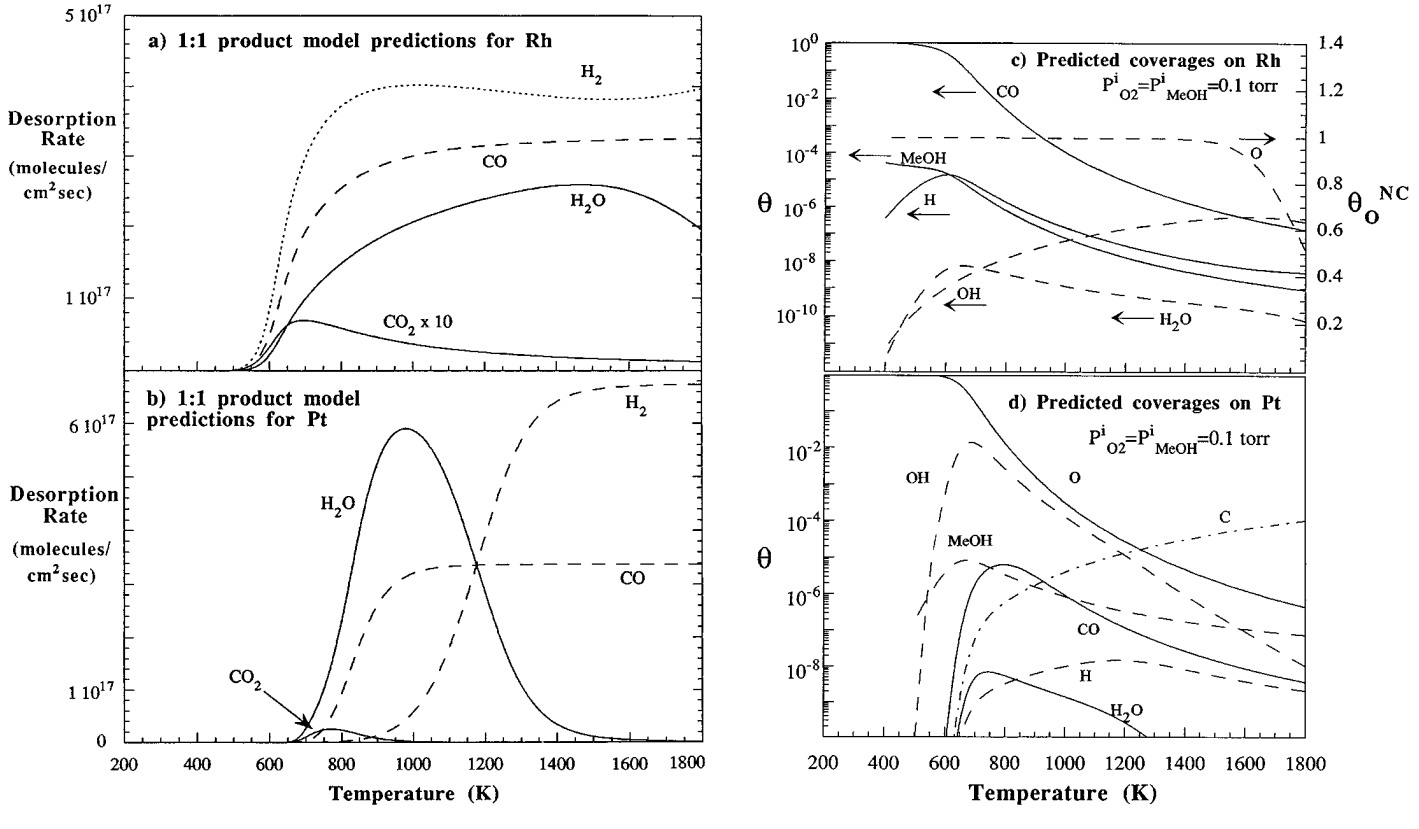

FIG. 6. Model predicted CO, CO_2, H_2, and H_2O desorption as a function of temperature for methanol oxidation (0.1 Torr MeOH; 0.1 Torr O_2) on (a) Rh and (b) Pt. Model predicted surface coverages as a function of temperature on (c) Rh and (d) Pt.

of 10 to show the qualitative trend more clearly. Therefore, the model considerably underpredicts CO_2 production. Unlike Pt, where oxygen competes with other species and thus excess methanol results in lowered CO_2 desorption, we find that increasing methanol partial pressure will increase CO_2 production as the noncompetitive oxygen coverage remains approximately constant. This phenomenon is also verified experimentally. We see more CO_2 desorbing from 0.1 Torr of methanol than for 0.03 Torr. At very high methanol partial pressure (0.3 Torr), CO_2 production decreases, probably because of oxygen binding equilibrium considerations. Specifically, excess methanol reduces competitive sites available for oxygen due to surface CO, and it is probably through these sites that oxidation occurs, not directly from the strongly bound noncompetitive sites. On Pt the CO_2 agreement is excellent, both in peak temperature placement and in peak magnitude.

The model prediction of CO shows excellent correlation to experiments over both Rh and Pt. Specifically, we see a substantial increase in CO production with increasing methanol. We also reach flux limited values for CO desorption at ~700–900 K, a result consistent with experiments.

Water and H_2 production are also summarized in Fig. 6. We see a substantial difference for these two products between Pt and Rh. Pt shows water and hydrogen production in two distinct zones, a phenomena which is also seen experimentally, but to a less obvious degree. Rh allows the two products to be produced simultaneously as seen experimentally. The noncompetitive nature of oxygen binding allows for high oxygen coverages and substantial water production, even at high temperatures. Note that the model predicts that water desorption from Rh is substantially lower than H_2 desorption ($\sim\frac{1}{2}$). In contrast, the model for Pt shows equal amounts of H_2O and H_2 desorption, with peak amounts occurring in different temperature regimes. This is consistent with the experimental fact that Rh desorbs substantially more hydrogen than Pt.

The major deficiency of the model for Rh occurs for methanol conversion in large excess oxygen ($>2:1$ O_2, not illustrated). The model fails to predict increases in the temperature at which measurable reaction begins with increasing oxygen partial pressure. This is believed to again relate to the dual nature of oxygen binding as the model currently allows oxygen in the high-energy binding state to react. Oxygen reaction from only the low-energy binding state might offer an interpretive improvement. The ratio of high/low binding state oxygen can be set as an equilibrium, as considered previously (1). Therefore, high oxygen partial pressures will force additional oxygen into competitive binding sites which can block the surface for methanol adsorption and decomposition at lower temperatures (500–800 K). This effect strongly contrasts with Pt, where oxygen addition helps remove built-up carbon and actually improves activity.

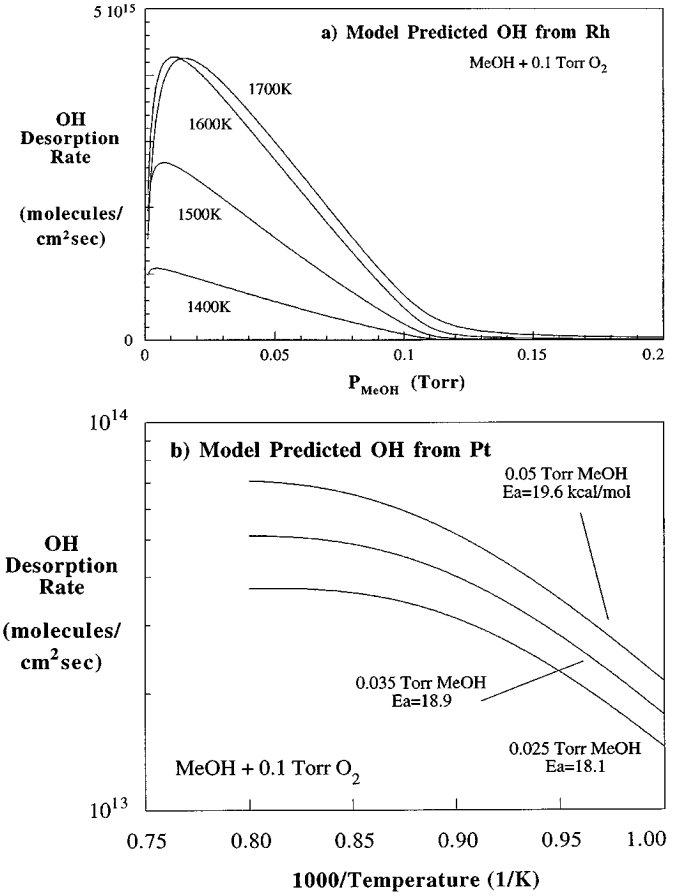

FIG. 7. (a) Model predicted results for OH desorption rate as a function of methanol pressure in 0.1 Torr O_2 over a Rh catalyst. (b) Model predicted results for OH desorption rate as a function of reciprocal temperature during methanol oxidation on Pt.

Figure 7a illustrates model prediction of OH desorption on Rh. At temperatures up to ~1700 K, the Rh model accurately predicts variations in OH desorption with increased methanol pressure and accurately shows the temperature dependence of OH desorption (Fig. 4a). The model predicts that rates level off above 1700 K, while we see an experimental increase in desorption up to the 2000 K limit of experiments.

Model predictions of OH desorption from Pt (Fig. 7b) also generally agree very well with experimental data (Fig. 4b), predicting the temperature-dependent apparent desorption activation barrier (the model predicts a range from 19.6 to 18.1 kcal/mol under conditions which are very close to the experimental average of 20 kcal/mol). The model predicted flux limit occurs at ~1200 K, while experimentally the limit occurs closer to 1400 K.

We should note that the models never predict oscillations (as seen experimentally on Pt). This is the result of the steady-state nature of the coverage balances. A transient

heat balance would need to be incorporated to allow accurate modeling of oscillatory behavior.

Coverages

Figure 6 also shows predicted coverages for the equimolar methanol oxidation system on Rh (c) and Pt (d). On Rh, noncompetitive oxygen remains extremely high (>0.5), even at 1800 K. As with methanol decomposition (not illustrated), CO remains the dominant competitively adsorbed species.

Overall, coverages in the Pt reaction system remain low at temperatures above ~1000 K in methanol decomposition (not illustrated) and ~700 K for oxidation (Fig. 6d). Since oxygen is the most stable surface species on Pt, it tends to quickly build up in oxidation, although it will readily recombine with adsorbed hydrogen to form water at temperatures above 700 K. In methanol decomposition (no oxygen present), carbon covers the surface below 800 K which leads to low activity.

Basic versus Carbon Model for Rh

A model allowing carbon formation was also able to predict methanol decomposition, but it offered no additional advantages over the simpler model *for Rh*. Parameter k_6 ($C_a + O_a \rightarrow CO_a$) was simply set so that pyrolyzed methanol would instantly recombine to surface CO and hydrogen, the net effect being similar to the basic model. This interpretation is consistent with prior work of Bowker (32), who indicates that Rh surface C and O will rapidly recombine relative to any minor CO dissociation. Furthermore, the surface-carbon model for Pt does *not* work well for methanol oxidation on Rh due to the extremely high binding energy of oxygen. Although oxygen does not directly interfere with methanol adsorption (oxygen primarily binds noncompetitively), the high oxygen coverage does not allow adsorbed methanol to decompose to surface carbon, oxygen, and hydrogen. This effectively shuts down the catalyst at temperatures below 1400 K, which is clearly not consistent with experimental results. Ot course, a surface-carbon model could be modified to allow oxygen from decomposed methanol to enter a competitive site first and affect the oxygen equilibrium between the two types of sites. However, this poses no significant advantage over maintaining our simpler model and keeping the methanol C–O bond intact on Rh.

DISCUSSION

Methanol Decomposition

Methanol decomposition on Rh shows carbon monoxide production at temperatures of 550 K and lower. This is believed to be indicative of a catalyst that is fully active, even at lower temperatures. Therefore, in contrast to Pt, we believe that the methanol decomposition route on Rh is through a surface methoxy species which maintains the integrity of the C–O bond, even at low temperatures.

On Pt, although we cannot say definitively why methanol decomposition is suppressed below 800 K in the absence of oxygen, we have speculated that this occurs because of carbon species build up on the catalyst surface. This theory is fairly well supported by our experimental evidence. Both Papapolymerou (4) and our current study found that methanol decomposition displays extremely strong deactivation above ~0.2 Torr methanol, making acceptable steady-state data acquisition "impossible." Furthermore, XPS indicates that an inactive catalyst surface contains >2 times more carbon than a comparable active surface.

Alternatively, we have considered the notion that carbon monoxide and not carbon, is poisoning the low temperature Pt surface. This is not consistent with low activity below 800 K; the 32 kcal/mol desorption barrier of CO results in significant CO desorption from Rh at temperatures as low as 600 K (as seen in Fig. 1a). The CO desorption barrier on Pt is 30 kcal/mol, lower than that for Rh, which should result in CO desorption at even lower temperatures than a comparable Rh catalyst. Furthermore, Seebauer has shown that a CO covered surface actually *lowers* this desorption activation barrier to 16 kcal/mol for coverages in excess of 0.5 monolayer (33). Therefore the notion of CO as a "poisoning" site blocker is not well supported.

One option that we will consider is that the carbon formed does *not* actually leave. This would indicate that we are really seeing either a decomposition reaction supported by a "carbon" catalyst (as overlayers on a Pt substrate) or some type of homogeneous decomposition reaction sustained through heat transfer from the catalyst surface into the gas phase. Experimentally, neither of these options is well-supported. In both cases, we would not expect to see any type of catalytic deactivation occur. In other words, we would expect to see the flux limited decomposition of methanol increase with methanol partial pressure, even at partial pressures above 0.2 Torr. Experimentally, the decomposition reaction cannot be sustained above 0.2 Torr as product partial pressures continually decrease, indicating that some type of deactivation *is* occurring.

Another possible explanation considers a change in the nature of the decomposition route of methanol on the Pt catalyst. Initially, it is fairly well understood that methanol bonds on Pt through the oxygen lone pair electrons (6, 17). From this adsorbed state, methanol has several *possible* routes by which to decompose. However, most conventional studies indicate that the preferential route of methanol decomposition is through the formation of a methoxy (CH_3O) intermediate and adsorbed hydrogen on Pt (6, 9, 11, 34) and Pd (22, 35). The majority of these studies offer temperature-programmed desorption (TPD)

data illustrating methanol desorption at ~140–180 K, followed by H_2 desorption at 360 K and CO desorption at ~470–540 K from a clean Pt surface. Discussion then follows that the adsorbed low-temperature methanol either desorbs or forms methoxy which is seen through TPD as desorbed CO and H_2 (there has been no evidence of *direct* desorption of methoxy (18)). Methoxy intermediate is strongly suggested by the absence of water as a desorption product. Several groups (7, 14, 36) have shown that another possible route of methanol decomposition exists which yields the formation of adsorbed *carbon* on a Pt surface, however. Specifically, Masel (7) has shown that different faces of Pt can yield substantially different TPD spectra, and further that some surface structures (2×1 Pt(110)) offer spectra indicative of surface methoxy formation while other structures (1×1 Pt(110)) yield results indicative of surface methyl (CH_3) formation which eventually leads to adsorbed surface carbon. Given this, although we believe that the "primary" route of methanol decomposition is through surface methoxy on polycrystalline Pt, we now theorize that adsorbed low temperature (<800 K) methanol is also significantly decomposed through breaking of the CH_3–OH bond. This interpretation is consistent with supporting evidence for the formation of methyl species on Pd (14) and Pt (7, 36). Overall, methyl formation initially results in a substantial amount of hydroxyl on the catalyst surface which will quickly scavenge hydrogen from the adsorbed methyl radical. This would briefly allow for some water production, but will inevitably cause a rapid deactivation of the catalyst surface due to coking by adsorbed CH_x species.

As the catalyst temperature reaches 800 K and above, however, the rate of CH_3–OH bond breaking decreases sufficiently relative to the primary decomposition route of CH_3O–H bond breaking to allow sustainable methanol decomposition. The formation of the "preferred" methoxy radical on the catalyst surface has the very important effect of keeping the C–O bond intact, and this bond will continue to strengthen on a Pt surface as surface methoxy undergoes hydrogen abstraction. Once stripped of all hydrogen (to form carbon monoxide), the C–O bond becomes completely nondissociative on the Pt catalyst (37). Thus, carbon does not have the opportunity to form on the surface with the overall effect of keeping the catalyst active for methanol decomposition above 800 K.

Of course, completely removing the CH_3–OH decomposition route above 800 K does not adequately explain all observed phenomena. For example, catalyst deactivation is still prevalent at high temperatures for $P^{i}_{MeOH} > 0.2$ Torr. We are sure that although CH_3O–H bond breaking becomes the *primary* route, it is not the only route of methanol decomposition. We believe that methanol will, in fact, continue to form some methyl and hydroxyl species and that this will continue to cause problems with coking, particularly at the higher methanol coverages associated with partial pressures >0.2 Torr.

The previous interpretation is generally consistent with the carbon model for methanol decomposition; carbon is by far the major surface species at all temperatures and comprises coverages in excess of 0.3 monolayers at temperatures below 800 K. Above this temperature, carbon surface coverage decreases sufficiently to allow methanol decomposition. The carbon model makes the simplifying assumptions that absorbed methyl or CH_x will be rapidly decomposed to surface carbon and hydrogen while surface methoxy will quickly decompose to form CO.

Methanol Oxidation

The oxidation reactions are interesting, both in the similarities and in the differences between Pt and Rh. For example, Rh offers no indication of oscillatory behavior. This is consistent with our interpretation that methanol's C–O bond is essentially nondissociative. As we indicated earlier, it is the presence of site-blocking carbon which causes Pt system oscillations. On Rh no carbon forms; therefore, no oscillations are seen.

Rh also show substantially more H_2 (and less H_2O) desorption than Pt at similar conditions. An examination of equal amounts of methanol and oxygen (0.1 Torr each, Fig. 2b versus Fig. 2e) illustrates that H_2 is the primary product over Rh, and H_2O is that over Pt. This is completely consistent with our previous analysis. We have shown by way of the potential energy diagrams for Pt and Rh (Fig. 8) that Pt energetically favors water production. Rh strongly favors desorption of H_2 over crossing the OH transition barrier to form H_2O.

On Pt, it is apparent from the data that even small dosages of oxygen can substantially lower the temperature of methanol conversion. This can be generally attributed to a surface oxygen recombination with adsorbed carbon, although it appears that surface carbon can still readily form at low temperatures and oxygen inlet pressures up to 0.1 Torr. However, the addition of small amounts of oxygen does serve to remove formed carbon from the catalyst, thus allowing the full range of the decomposition "zone" to become apparent. In other words, the methyl formation route which dominates at temperatures below 800 K now has a ready pathway by which to react and desorb by reaction with oxygen. This offers some explanation for why conversion temperatures drop dramatically as oxygen partial pressure increases; the additional oxygen can keep the foil "clean" at lower temperatures. This is only a partial explanation, however; additional oxygen also promotes production of complete combustion products, which tend to desorb at a much lower temperatures.

Although literature examining methanol oxidation is generally limited to low temperature TPD of adsorbed methanol on an oxygen precovered Pt of Pd surface (5, 9,

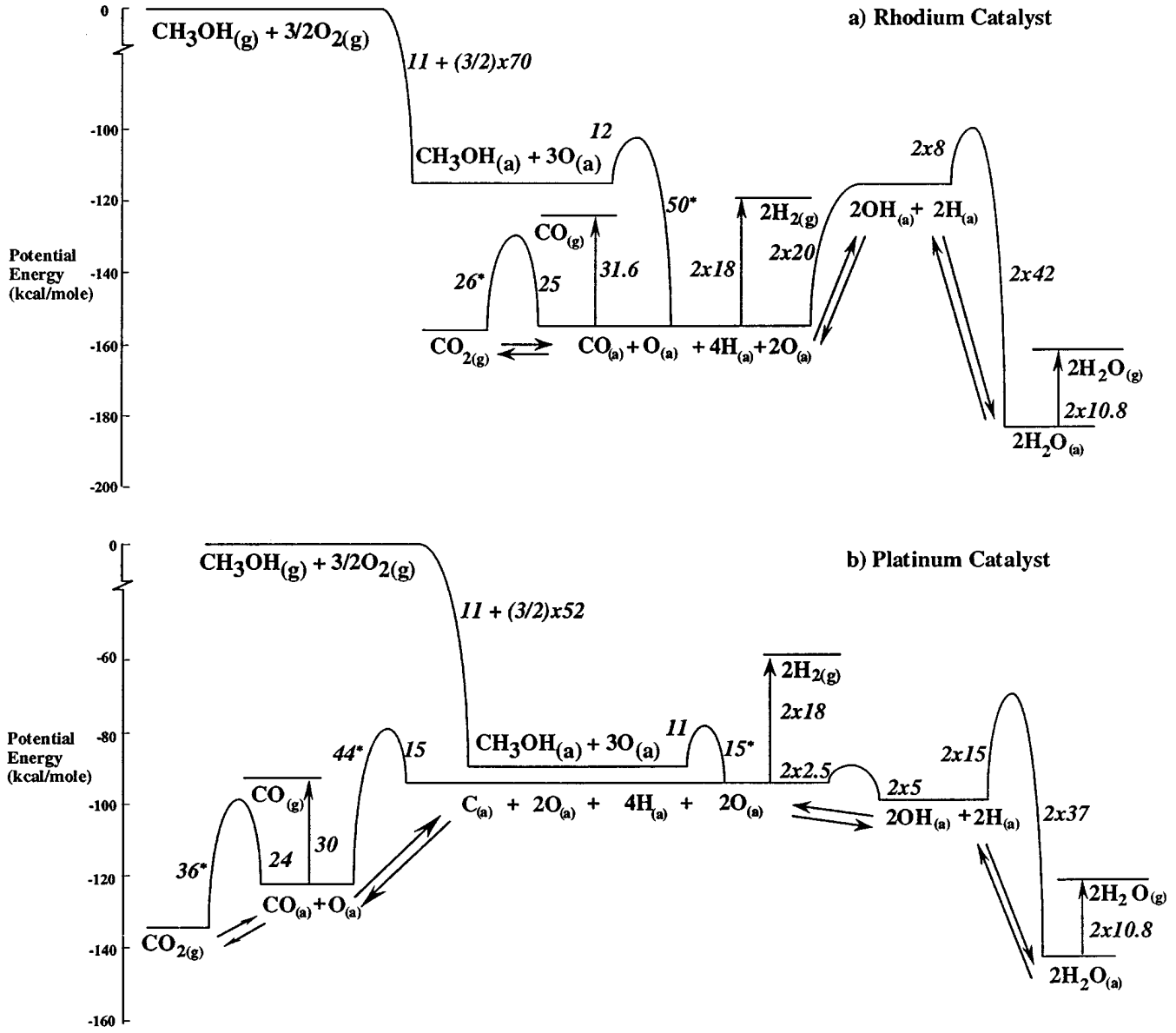

FIG. 8. Potential energy diagrams for methanol oxidation on a (a) Rh and (b) Pt catalyst. Asterisks designate activation barriers closed by thermodynamic constraints.

21, 22, 24, 35) Schäfer and Wassmuth (38) noted several interesting results in a study of carbon oxidation on a Pt surface. Specifically, they note that carbon is removed at temperatures from 450 to 700 K as CO_2 and that desorption of carbon as CO can occur at temperatures in excess of 700 K. Furthermore, CO_2 desorption shifts in temperature with increasing carbon coverage. Desorption can occur at temperatures as low as 450 K on a clean Pt surface, but CO_2 desorption tends to shift up to 650 K as surface carbon coverage becomes large. They note that the dominant desorption product for carbon oxidation is CO_2 at temperatures under 700 K and CO at temperatures above 700 K. Finally, they indicate that molecular oxygen desorption begins significantly at ~750 K. This offers an additional explanation for the transition to CO, as oxygen is being removed from the system via desorption above 750 K. This is also consistent with results of Campbell *et al.* (25), who note that the desorption barrier for CO recombination with O on Pt (reaction k_5) can drop from 24 kcal/mol to as low as 11 kcal/mol as oxygen coverage approaches 1.0 monolayer. This shift in activation barrier will result in lowered desorption temperatures for CO_2 products. Model based analysis indicates that oxygen coverage does in fact approach 1.0 monolayer on Pt at a temperature of 600 K (Fig. 6d).

The results of our study of methanol oxidation are consistent with this analysis. We can see conversion on Pt

beginning as low as 450 K in large excess oxygen, as shown previously by McCabe (23, 39) for fuel-lean methanol oxidation on Pt coated alumina. This is also consistent with CO_2 formation on a clean catalyst surface as shown by Schäfer. As oxygen decreases in the system, CO + O combination and desorption shifts up to 650 K, again consistent with the oxidation results of Schäfer. Overall, our data indicate that the methanol reaction in these cases is limited by CO + O combination and desorption. As oxygen continues to decrease, we see that the methanol conversion slope decreases and correspondingly, the oxidation to CO_2 slows down. Concurrent with that, we see a decrease in methanol conversion. By ~800 K, product desorption shifts somewhat as oxygen begins to desorb molecularly and CO is produced.

An examination of product partial pressures also illustrates the changing region of reaction (Fig. 2). Figure 2d shows excess methanol on Pt; this leads directly to CO which does not desorb at lower temperatures, even on a clean Pt catalyst. Excess oxygen (Fig. 2f) yields almost exclusively CO_2 and water which *will* desorb at low temperatures. Under these conditions, we believe that the surface remains sufficiently oxygenated to offer complete combustion, even at the high temperature experimental limits. Equal inlet pressures of methanol and oxygen (Fig. 2e) result in low temperature CO_2 evolution, followed by CO and water desorption above the oxygen desorption temperature of 800 K. Initially, water production appears to be inconsistent with the formation of low temperature total oxidation products; however, note that the maximum product pressure for CO_2 is only ~0.001 Torr. Unlike CO_2, which is extremely sensitive (<0.0001 Torr resolution) in mass spectrometer analysis, water is not. Therefore, it is likely that water desorption at low temperatures is also on the order of 0.001 Torr (to preserve mass balance), but this is effectively below our sensitivity to detect changes in mass 18-peak characteristics. Finally, above 800 K CO formation is expected, and water formation is consistent with the formation of hydroxyl surface species during CH_3–OH bond breaking.

It is interesting to note that combustion and decomposition products appear to come off in two distinct reaction "zones." The decomposition zone occurs at temperatures above 800 K. In contrast, the oxidation zone can occur at temperatures as low as 450 K. This is most readily apparent in the figures of product partial pressures versus temperature (Figs. 4, 5b, 5d and 5f). CO_2 and H_2O products obviously leave the Pt surface at significantly lower temperatures than either CO or hydrogen. This is also indicated strongly by the model analysis, we can see that CO_2 and H_2O come off at significantly lower temperatures than CO and H_2. The rationale is twofold; we see larger oxygen coverages at lower temperatures, coupled with lower desorption barriers for the oxidation species.

We should note that product partial pressures for equal mixtures of methanol and oxygen are somewhat unexpected in terms of reaction thermodynamics. Specifically, we see substantially more water produced than hydrogen. Thermodynamically, we might expect equal amounts of water and hydrogen. As we have indicated previously, however, hydrogen and oxygen tend to form water readily and desorb from the Pt surface. This is generally favored over desorption of unreacted hydrogen on Pt and may offer some explanation for water as a favored product when sufficient oxygen is available on the catalyst surface.

Fluorescence conducted on Rh indicates a peak OH production in very strong excess oxygen (0.1 Torr oxygen, <0.01 Torr methanol). This result is also consistent with the extreme transition barrier of hydrogen oxidation. Substantial excess oxygen is necessary to overcome the oxygen's 70 kcal/mol binding energy (40) and generate surface hydroxyl which can be viewed through LIF.

Finally, we can view mechanistic results by way of a potential energy diagram for the Rh and Pt methanol system (Fig. 8). This diagram graphically illustrates the mechanistic parameters chosen in our basic model interpretation of methanol decomposition and oxidation reactions on this catalyst surface. We believe the most substantial differences between Pt and Rh still stem from the nature of adsorbed OH and its activation barrier to water formation on Rh, a result which directly carries over from our analysis of the hydrogen oxidation system (1). Some barrier heights are set by thermodynamic constraints (noted with asterisks).

Oscillations on Pt

We have noted oscillation in temperature, reactant, and product partial pressures on the Pt system. There are many possible reasons for the oscillations found in the Pt reaction system, several examples are given in a review by Schmidt *et al.* (41). One of the best known reactions for oscillations on Pt in this pressure regime is the bimolecular CO oxidation reaction. A fairly comprehensive review of this specific reaction was give by Razon and Schmitz (42). This reaction has a well-documented variation in CO oxidation to CO_2 in time under a variety of CO/O_2 partial pressures.

Although a bimolecular oxidation reaction of this sort certainly appeals to our current reaction system and CO/oxygen oscillations are possible in this reaction system, all reported instances of oscillations in this reaction occur at fairly low temperatures (the absolute maximum reported is ~600 K). This temperature range makes it apparent that CO/O_2 oscillations result in some fashion from a high CO coverage, as the 30 kcal/mol CO desorption barrier keeps the molecule tightly bound to a Pt surface below 600 K. This is also far below the temperature range where we see oscillatory behavior in the methanol system. Of course, this does not preclude the possibility of some other bimolecular combination giving rise to this type of oscillatory behavior,

but it does lead us to consider the notion of a methanol unimolecular oscillation system as described below.

Previously, Cordonier (43) has shown the existence of oscillations in unimolecular methyl amine decomposition. Due to similarities between methanol (CH_3OH) and methyl amine (CH_3NH_2), it is reasonable to consider the possibility that methanol oscillations are primarily driven by unimolecular forces. This is not an obvious first choice given the presence of oxygen in our reaction system, but it does follow strongly from the theories outlined below. Basically, we believe that the decomposition of methanol to surface CH_3O and H is the dominant reaction in the range of oscillatory temperatures (consistent with the above decomposition analysis). Alternatively, however, CH_3 and OH *can* form at these same temperatures. Then the carbon containing methyl species serves as a reaction site "blocker" and this can yield oscillatory behavior as surface intermediate concentrations shift between CH_3O and CH_3. This interpretation is consistent transition from an inactive (CH_3 blocked) to an active (CH_3O covered) catalyst surface which we see over the same temperature range in methanol decomposition. Furthermore, this explanation is analogous to that for oscillations in methyl amine decomposition (43) (although the active and site-blocking species are HCN and CN, respectively), and the methyl amine reactions occur on polycrystalline Pt at the same pressure and temperature range as for methanol.

The undesirable aspect of explaining methanol oscillations in terms of a unimolecular reaction route is that we obviously require the presence of oxygen in the reaction system for oscillations to occur. This would generally be interpreted as consistent with a bimolecular reaction, not a decomposition. This can be explained in terms of a necessary oxygen minimum to maintain surface cleanliness, however. Zero surface oxygen results in no surface oscillation because an inactive or carbon covered surface cannot "regenerate" activity. Intermediate oxygen pressures allow a unimolecular C/CO competition, but also keep carbon levels low enough through oxidation routes to maintain catalyst activity. At the other extreme, adding excessive amounts of oxygen (pressure above ~0.11 Torr) completely removes CH_x as a surface intermediate and thus effectively eliminates any oscillatory behavior. Therefore surface oxygen plays an important, although indirect, role in this unimolecular oscillation. Cordonier also noted periodic deactivation in the methyl amine oscillations and found that the addition of oxygen had no influence on his observed oscillatory reaction dynamics.

Finally, it is apparent that this behavior occurs in the temperature range that corresponds to a shift from the "oxidation zone" to the "decomposition zone." We believe that this connection is very important and that these oscillations are strongly linked to the shift from surface oxidation to surface decomposition. Although speculative on our part, this is consistent with a transition from adsorbed CH_3O to CH_3 with methyl serving as a site blocker. Nevertheless, the actual mechanism remains unknown.

SUMMARY

From the results and models, we conclude the following:

(1) The decomposition of methanol on polycrystalline Pt is strongly inhibited by the formation of adsorbed carbon. Above 800 K, methanol decomposes primarily through an adsorbed methoxy species, which keeps the methanol C–O bond intact and the catalyst surface active. This contrasts strongly with Rh, where the methanol C–O bond appears to be nondissociative at all temperatures.

(2) Oxygen behaves differently on the two metal surfaces. The strong binding of oxygen on Rh suppresses low temperature reactions at high P_{O_2} due to site competition. In contrast, additional oxygen results in further activation of Pt (i.e., allows conversion at lower temperatures) since carbon is the primary site-blocker. Oxygen removes surface carbon and increases CH_3OH activity on Pt so that rates on Pt and Rh are comparable.

(3) We have demonstrated that oxidation products generally evolve in two different regimes on Pt. Complete combustion products desorb at temperatures from 450–700 K while decomposition products are seen primarily above 700 K, along with increased oxygen desorption. On Rh, oxygen tends to bind strongly even at high temperatures, and therefore, the oxidation zone extends up to the 1600 K limit of experiments.

(4) Based on the conditions encountered for oscillatory behavior, we believe that Pt oscillations are driven primarily through competing unimolecular decomposition pathways. Specifically, oscillations are the result of methanol decomposition to methoxy in competition with the decomposition to methyl (a site-blocker). This interpretation is consistent with previous results shown for methyl amine. On Rh, no oscillations in reactant partial pressure, product partial pressure, or temperature are noted, which is also consistent with our unimolecular theory of methanol oscillation on Pt. Carbon is not available to block sites on the Rh surface during this reaction and generate oscillatory behavior.

(5) Under equimolar oxygen and methanol conditions (partial oxidation), Rh generally favors H_2 desorption, unlike Pt which favors H_2O desorption. This is consistent with our previous research on hydrogen oxidation, where we find that the high activation barrier to water formation of Rh results in an energetic preference for surface hydrogen to desorb as H_2 rather than oxidize to H_2O.

(6) A simple mechanistic analysis which considers the possibility of carbon formation from methanol on Pt and the nondissociative nature of methanol C–O bond on Rh gives an excellent qualitative prediction of experimental results.

APPENDIX: NOMENCLATURE

$O_{(a)}$, $H_{(a)}$, $OH_{(a)}$, $C_{(a)}$, $H_2O_{(a)}$, $CO_{(a)}$, $MeOH_{(a)}$	adsorbed (surface) species
k_{aM}, k_{aO}	adsorption rates of methanol and O_2 ($Torr^{-1}\ s^{-1}$)
k_{dH}, k_{dO}, k_{dW}, k_{dOH}, k_{dM}, k_{dCO}	desorption rates of H, O, H_2O, OH, MeOH, and CO (s^{-1})
k_i, k_{-i}	rate constant of forward and reverse reaction i (s^{-1})
$P^i_{O_2}$, P^i_{MeOH}	inlet CSTR pressures of O_2 and MeOH (no reaction)
P_{O_2}, P_{MeOH}	CSTR pressures of O_2 and MeOH with reaction
θ	surface coverage (competitive)
θ_v	coverage of vacant sites
$\theta_o^{(NC)}$	coverage of noncompetitive oxygen
n	oxygen adsorption/desorption and hydrogen desorption order
E_A	activation energy
T_s	surface temperature
T_g	gas temperature
$V_{r\times r}$	reactor volume
$A_{surface}$	catalyst surface area
N_{av}	Avagadro's number
τ	species residence time
N_o	monolayer coverage
f	oxygen binding state ratio
R	ideal gas constant
S	sticking coefficient
m	molecular weight

ACKNOWLEDGMENT

This research supported by DOE under Grant DE-FG02-88ER13878-A02.

REFERENCES

1. Zum Mallen, M. P., Williams, W. R., and Schmidt, L. D., *J. Phys. Chem.* **97**, 625 (1993).
2. Williams, W. R., Marks, C. M., and Schmidt, L. D., *J. Phys. Chem.* **96**, 5922 (1992).
3. Cheng, W., and Kung, H. H., "Methanol Production and Use." Dekker, New York, 1994.
4. Papapolymerou, G. A., and Schmidt, L. D., *Langmuir* **3**, 1098 (1987).
5. Kizhakevariam, N., and Stuve, E. M., *Surf. Sci.* **286**, 246 (1993).
6. Attard, G. A., Chibane, K., Ebert, H. D., and Parsons, R., *Surf. Sci.* **224**, 311 (1989).
7. Wang, J., and Masel, R. I., *Surf. Sci.* **243**, 199 (1991).
8. Wang, J., and Masel, R. I., *J. Vac. Sci. Technol.* **A9**, 1879 (1991).
9. Sexton, B. A., *Surf. Sci.* **102**, 271 (1981).
10. Gibson, K. D., and Dubois, L. H., *Surf. Sci.* **233**, 59 (1990).
11. Redulic, K. D., and Sexton, B. A., *J. Catal.* **78**, 126 (1982).
12. Parmeter, J. E., Jiang, X., and Goodman, D. W., *Surf. Sci.* **240**, 85 (1990).
13. Kruse, N., Chuah, G.-K., Abend, G., Cocke, D. L., and Block, J. H., *Surf. Sci.* **189/190**, 832 (1987).
14. Levis, R. J., Zhicheng, J., and Winograd, N., *J. Am. Chem. Soc.* **111**, 4605 (1989).
15. Kruse, N., Rebholz, M., Matolin, V., Chauh, G. K., and Block, J. H., *Surf. Sci.* **238**, L457 (1990).
16. Bhattacharya, A. K., Chesters, M. A., Pemble, M. E., and Sheppard, N., *Surf. Sci.* **206**, L845 (1988).
17. Davis, J. L., and Barteau, M. A., *Surf. Sci.* **187**, 387 (1987).
18. Christmann, K., and Demuth, J. E., *J. Phys. Chem.* **76**, 6318 (1982).
19. Christmann, K., and Demuth, J. E., *J. Phys. Chem.* **76**, 6308 (1982).
20. Davis, J. L., and Barteau, M. A., *Surf. Sci.* **235**, 235 (1990).
21. Gates, Kesmodel, *J. Catal.* **83**, 437 (1983).
22. Hartmann, N., Esch, F., and Imbihl, R., *Surf. Sci.* **297**, 175 (1993).
23. McCabe, R. W., and McCready, D. F., *J. Phys. Chem.* **90**, 1428 (1986).
24. Akhter, S., and White, J. M., *Surf. Sci.* **171**, 527 (1986).
25. Campbell, C. T., Ertl, G., Kuipers, H., and Segner, J., *J. Chem. Phys.* **73**, 5862 (1980).
26. Ehsasi, M., Matloch, M., Frank, O., Block, J. H., Christmann, F. S., Rys, F. S., and Hirschwald, W., *J. Chem. Phys.* **91**, 4949 (1989).
27. Matsushima, T., *Surf. Sci.* **127**, 403 (1983).
28. Marks, C. M., and Schmidt, L. D., *Chem. Phys. Lett.* **178**, 358 (1991).
29. Dieke, G. H., and Crosswhite, H. M., *J. Quant. Spectrosc. Radiat. Transfer* **2**, 97 (1962).
30. Root, T. W., Schmidt, L. D., and Fisher, G. B., *Surf. Sci.* **134**, 30 (1983).
31. Wagner, M. L., and Schmidt, L. D., *J. Phys. Chem.* **99**, 805 (1995).
32. Bowker, M., *Catal. Today* **15**, 77 (1992).
33. Seebauer, E. G., Kong, A. C. F., and Schmidt, L. D., *Surf. Sci.* **176**, 134 (1986).
34. Peremans, A., Maseri, F., Darville, J., and Gilles, J.-M., *Surf. Sci.* **227**, 73 (1990).
35. Jorgensen, S. W., and Madix, R. J., *Surf. Sci.* **183**, 27 (1987).
36. Levis, R. J., Zhicheng, J., Winograd, N., Akhter, S., and White, J. M., *Catal. Lett.* **1**, 385 (1988).
37. Horn, K., Bradshaw, A., and Jacobi, K., *Surf. Sci.* **72**, 719 (1978).
38. Schäfer, L., and Wassmuth, H.-W., *Surf. Sci.* **208**, 55 (1989).
39. McCabe, R. W., and Mitchell, P. J., *Appl. Catal.* **27**, 83 (1986).
40. Matsushima, T., *Surf. Sci.* **157**, 297 (1985).
41. Schüth, F., Henry, B. E., and Schmidt, L. D., *Adv. Catal.* **39**, 51 (1993).
42. Razon, L. F., and Schmitz, R. A., *Catal. Rev.–Sci. Eng.* **28**, 89 (1986).
43. Cordonier, G. A., Schüth, F., and Schmidt, L. D., *J. Chem. Phys.* **91**, 5374 (1989).
44. Campbell, C. T., Shi, S. K., and White, J. M., *J. Phys. Chem.* **83**, 2255 (1979).
45. Yates, J. T., Thiel, P. A., and Weinberg, W. H., *Surf. Sci.* **84**, 427 (1979).
46. Kiss, J., and Solymosi, F., *Surf. Sci.* **177**, 191 (1986).
47. Wagner, F. T., and Moylan, T. E., *Surf. Sci.* **191**, 121 (1987).
48. Thiel, P. A., and Madey, T. E., *Surf. Sci. Rep.* **7**, 211 (1987).
49. Hickman, D. A., and Schmidt, L. D., *AIChE J.* **39**, 1164 (1993).
50. Sexton, B. A., Rendulic, K. D., and Highes, A. E., *Surf. Sci.* **121**, 181 (1982).
51. McCabe, R. W., and Schmidt, L. D., *Surf. Sci.* **65**, 189 (1977).
52. Fisher, G. B., and Gland, J. L., *Surf. Sci.* **94**, 446 (1980).